UC Berkeley
Earlier Faculty Research

Title
A Car-Following Theory for Multiphase Vehicular Traffic Flow

Permalink
https://escholarship.org/uc/item/9m6307tb

Authors
Zhang, H. Michael
Kim, T.

Publication Date
2003-09-01

A car-following theory for multiphase vehicular traffic flow[*]

H.M. Zhang [†]and T. Kim [‡]
Department of Civil and Environmental Engineering
University of California, Davis
Davis, California 95616

Abstract

We present in this paper a new car-following theory that can reproduce both the so-called capacity drop and traffic hysteresis, two prominent features of multiphase vehicular traffic flow. This is achieved through the introduction of a single variable, driver response time, that depends on both vehicle spacing and traffic phase. By specifying different functional forms of response time, one can obtain not only brand new theories but also some of the well-known old car-following theories, which is demonstrated in this paper through both theoretical analyses and numerical simulation.

1   INTRODUCTION

Various theories attempt to describe the vehicular traffic flow process. One class of such theories, called car-following theories, is based on the follow-the-leader concept, in which rules of how a driver follows his/her immediate leading vehicle are established based on both experimental observations and theoretical (i.e., psychological) considerations. Existing theories of this kind were shown to capture some of the qualitative features of traffic flow, such as the backward propagation of traffic disturbances through a line of vehicles and traffic instability. Yet they fall short in modeling some prominent traffic flow features, namely the so-called capacity drop and traffic hysteresis, both are clearly observable from experimentally obtained flow-density, flow-speed or speed-density plots [1]. The former was first noticed by Eddie [4] who observed a sharp speed drop in a small density range in some observed speed-density phase plots, and proposed a two-regime phase diagram to model it. The most important feature of this two-regime model is that the maximum flow rate achievable in congested traffic is lower than that in free flow traffic and this 'capacity drop' occurs suddenly in a certain density range. A multitude of studies has also reported this capacity drop as a consistent feature of congested traffic e.g. Koshi et al. [14]. The other important feature, traffic hysteresis, was recognized theoretically as early as 1965 by Newell [17], who speculated that drivers behave differently in different traffic phases, and built a multiphase traffic theory to explain instability in traffic. This theory,

---

[1]These plots, also known as phase diagrams, depict the pair-wise relations between the macroscopic traffic flow variables of flow, density, and speed.

however, does not model the capacity drop. The earliest, and perhaps the best known, experimental observations of traffic hysteresis are from Treiterer and Myers [20], while recent observations of this phenomena were reported in Zhang [21].

Both the capacity drop and traffic hysteresis are important because the former has profound implications to traffic control and the latter is intrinsically linked to stop-and-go traffic. Yet, no traffic theory up-to-date can describe both features. Although there are recent developments, namely the behavioral traffic wave theory of Daganzo [5] and the multiphase theory of Kerner [13], that made headway toward a unified traffic theory that can explain many important traffic features, these theories can model one of the two aforementioned phenomena but fall short in explaining both phenomena simultaneously. In this paper we make an attempt to develop a car-following theory that can describe both.

The remaining parts of the paper are organized as follows. First we shall review the link between congested traffic, steady-state phase diagrams and car-following theory in Section 2, then we develop the new car-following theory and discuss its qualitative features on a case by case basis in Section 3, and in Section 4 we present numerical simulation results. Finally we conclude the paper in Section 5.

2 FEATURES OF CONGESTED TRAFFIC AND CAR-FOLLOWING

Regardless of the cause of congestion, congested traffic usually exhibits two prominent features: 1) an initial front that induces sharp flow/density/speed changes, and 2) a prolonged period of stop-and-go motion across the congested region after the front passes. Viewed in the phase plane, these features translate into flow-density or speed-density or flow-speed jumps near a critical density/speed/flow region and periodic orbits, or hysteresis loops, in the high density or low speed region.

Eddie [4], from Lincoln Tunnel data, first noticed the existence of jumps in the density-speed scatter plot and hypothesized that speed-density or flow-density phase plots have two disjoint branches—one for free-flow traffic and the other for congested traffic, with the maximum flow of free-flow branch considerably higher than that of the congested branch, hence the name "capacity drop". Eddie noted that this jump in flow/speed could be an intrinsic property of vehicular traffic flow. Drake et al. [7] applied the two-regime hypothesis to traffic data and found that it produced the best fit with lowest standard error. Other experimental evidence of the existence of the "capacity drop" is from Japanese and German highways. Koshi et al. [14] analyzed traffic data from the Tokyo Expressway and found that their flow-density plots resembles 'the mirror image of a reversed λ' (Fig 1 (a)), with data points scattered more widely near the right leg of the reversed λ. Kerner [13], on the other hand, have shown that in German data the flow rate out of a wide jam is considerably lower than the maximal possible flow rate in free flow and a multitude of homogeneous states of synchronized flow covers a broad region around the characteristic line J (Fig.1(b)).

The first clear experimental evidence of traffic hysteresis was provided by Treiterer and Myers [20]. These authors studied a platoon of vehicles and estimated their average flow, density and travel speed. They found that both the flow-density and speed-density plots have loop structures. Other experimental evidence of traffic hysteresis include the observations of Maes [15] on Belgian highways and Zhang [21] on California highways.

Zhang [21] also noted the linkage between hysteresis and stop-start waves and provided a traffic theory to model it. The first exploitation of traffic hysteresis, however, is by Newell [17], who hypothesized that drivers respond to stimulus differently in acceleration and deceleration and developed a model that contains hysteresis loops (Fig 2) [2] Newell's hypothesis on driver behavior was corroborated by experimental observations of Forbes [8], who observed that a sudden change in drivers' response time occurs before and after a sudden deceleration. Forbes further suggested that this sudden change of response time explains the jumps found on various phase diagrams and proposed flow-density diagrams with multiple branches(Fig. 3).

Conventional traffic stream models (i.e., flow-density or speed-density diagrams or formulas), on the other hand, are usually described by continuous or even smooth functions that contain neither jumps nor hysteresis loops. Starting from the earliest to the latest, these models are smooth curves of linear (Greenshields [12]):

$$v = v_f - c_1\rho, \tag{1}$$

logarithmic (Greenberg [11]):

$$v = c_2 \ln\left(\frac{\rho_j}{\rho}\right) \tag{2}$$

exponential (Newell [16])

$$v = v_f \left[1 - \exp\left\{-\frac{\lambda}{v_f}\left\{\frac{1}{\rho} - \frac{1}{\rho_j}\right\}\right\}\right] \tag{3}$$

or other nonlinear forms (Del Castillo and Benetez [6]). The variables in these models are: v-traffic speed, v_f-free flow travel speed, c_1, c_2-constant parameters, ρ-traffic density, ρ_j-jam density, λ-the slope of the spacing-speed curve at $v = 0$.

A common property of these models is that most of these functions can be derived from one car-following model or another under steady-state traffic conditions, which provides them some behavioral and theoretical foundation. Both the Greenshields and the Greenberg traffic stream models are derivable from a car-following model of the form

$$\ddot{x}_n(t + T) = \alpha \frac{\dot{x}_n^l(t)}{(x_{n-1}(t) - x_n(t))^m}(\dot{x}_{n-1}(t) - \dot{x}_n(t)) \tag{4}$$

that is generally associated with research from the General Motors Laboratories [2, 9, 10]. If one adopts $l = 0$ and $m = 2$, one can obtain Greenshields model, and Greenberg's model if one adopts $l = 0$ and $m = 1$. Newell's traffic stream model, on the other hand, can be obtained from this car-following theory

$$\dot{x}_n(t + T) = v_f[1 - e^{-\frac{\lambda}{v_f}(x_{n-1}(t) - x_n(t) - L)}]. \tag{5}$$

The fact that these car-following models lead to smooth flow-density or speed-density relations attest, to a certain degree, their inadequacy to model complex traffic flow patterns that exhibit capacity drops and hysteresis loops. This is not surprising if one considers that conventional car-following models treat both drivers and roads as homogeneous entities— that is, they are modeling identical drivers who travel on homogeneous roads. The traffic

---

[2]The dotted lines in the figure represent the transient state that the follower wait until a gap is obtained to accelerate(lower dotted line) or decelerate (upper dotted line).

that produces capacity drops and hysteresis loops, on the other hand, comprise diverse groups of drivers who travel on inhomogeneous roads and may behave differently under different driving conditions. A plausible car-following theory that explains these nonlinear phenomena must consider these inhomogeneities. In the next section we shall develop such a theory.

3 A NEW CAR-FOLLOWING MODEL

Before developing the new car-following theory, we shall review an early theory by Pipes [19]. This would help explaining some of the basic notions of the new theory. Pipes car-following theory is a linear model that describes traffic behavior if drivers observe the driving rules suggested in the California Motor Vehicle Code—leave one car length in front for every ten miles/hour of speed increment, and has the following form:

$$x_{n-1} = x_n + b + \tau v_n + L \tag{6}$$

where, b is the legal distance between the vehicles at standstill, τ is a time constant, and L is the length of the leader vehicle. Let $L' = b + L$ and rewrite the equation as

$$v_n = \frac{1}{\tau}(x_{n-1} - x_n - L') = \frac{s_n}{\tau} \tag{7}$$

This will lend a new interpretation of Pipes' model: the follower adopts a speed of $\frac{s_n}{\tau}$, i.e., the vehicle spacing divided by a time-gap, or driver response time, as we shall call it.

Rather than using a constant driver response time, we shall propose that it is a function of both vehicle spacing and traffic phase, i.e., $\tau = h_n(t) = H[s_n(t), \mathcal{P}(t)]$, and suggest a new car-following model for multiphase flow as follows

$$\dot{x}_n(t + T) = \frac{s_n(t)}{h_n(t)} \tag{8}$$

where traffic phase $\mathcal{P}$ includes acceleration, deceleration and coasting, $\dot{x}_n(t + T)$ is the speed of nth vehicle at time t+T, T is driver reaction time [3].

By specifying different forms for the function H, we obtain various specific car-following models, among which some were discussed earlier in the text and some are brand new models that can reproduce either the capacity drop or traffic hysteresis or both phenomena. Below we discuss four such models and pay special attention to their steady-state phase diagrams, the flow-density diagram in particular, and compare them with known results.

3.1 Model A

In the first case we suggest that h be a linear function of vehicle spacing and independent of traffic phase

$$h_n(t) = h_0 + \frac{1}{v_f} s_n(t) = h_0 + a s_n(t) \tag{9}$$

where $v_f = \frac{1}{a}$ and h_0 are constants. This function is shown in Fig. 4(a)).

---

[3]Note that driver reaction time differs from driver response time, The minimum of latter is the former.

Under steady state conditions, where vehicular speed does not change, one has $\dot{x}_n(t + T) = v$ and $s_n(t) = S = \frac{1}{\rho} - \frac{1}{\rho_j}$. Here we used the facts that $s = \frac{1}{\rho}$ and $L = \frac{1}{\rho_j}$. Thus (8) with (9) reduces to

$$v = \frac{\frac{1}{\rho} - L}{h_0 + a(\frac{1}{\rho} - L)} = \frac{1 - L\rho}{h_0\rho + a - aL\rho}, \tag{10}$$

and the flow function is

$$q = \rho v = \frac{\rho - L\rho^2}{h_0\rho + a - aL\rho}. \tag{11}$$

Note that

$$v' = \frac{-h_0}{(a + h_0\rho - aL\rho)^2} < 0 \tag{12}$$

travel speed decreases with the increase of density. The properties of (11) are

1. **boundary conditions**

    1. $q = 0$ when $\rho = 0$ or $\rho = \rho_j = \frac{1}{L}$

    2. $q'_{\rho=0} = \frac{1}{a} = v_f$, $q'_{\rho=\rho_j} = -\frac{L}{h_0}$

2. **concavity** $q''(\rho) < 0$, and

3. **criticality** $\exists \rho_0 \in [0, \rho_j]$, s.t. $q \leq q(\rho_0)$, here $\rho_0 = \frac{aL \pm \sqrt{aLh_0}}{aL^2 - L\ h_0}$

which meets all the basic requirements of an equilibrium flow-density relationship (also known as the fundamental diagram of traffic flow) (Del Castillo and Benetize [6]). A specific case of this fundamental diagram is drawn in Fig. 4 (b) and compared with Greenberg's and Newell's fundamental diagrams in Fig. 5. The parameters used to draw these figures are L=6m, h_0=1sec, v_f=108km/hr, for model A, $\lambda = 0.833\text{sec}^{-1}$, and v_f=108km/hr for Newell's model, c_2=28km/hr and ρ_j=166veh/km.

Clearly, like other car-following models that do not distinguish traffic phases, this model produces neither the capacity drop nor hysteresis.

3.2 Model B

In this model, we hypothesize that drivers drive differently in free-flow and congested flow, and define the following $h_n(t)$ function:

$$\begin{aligned} h_n(t) &= \frac{s_n(t)}{v_f}, &\text{for } S_0 \leq s_n(t) \\ &= h_0, &\text{for } 0 \leq s_n(t) < S_0 \end{aligned}$$

where congested traffic occurs in $0 \leq s_n(t) < S_0$ and free-flow traffic in $S_0 \leq s_n(t)$. The fundamental diagram derived from this model is shown in Fig. 6(b), a triangle that is advocated by the Berkeley school of thought and derivable from Newell's lower-order car-following model [18]. Note that the triangular diagram satisfies both the concavity and criticality conditions and has physically meaningful parameters v_f, ρ_0 and ρ_j.

Although Model B still does not produce the capacity drop and traffic hysteresis in its fundamental diagram, its diagram shows some interesting new features, namely the loss of smoothness at the tip of the diagram (or at capacity flow) and the existence of two constant wave speeds. Both features imply that traffic waves produced on either branch of the diagram will not focus or expand, or the trajectory of a following vehicle is simply the translation of the trajectory of its leading vehicle some time later.

3.3　Model C

In this case we revise the response time function of Model B to include a transition region $[S_0, S_1]$ (see Fig. 7(a)). Outside of $[S_0, S_1]$, $h_n(t)$ is given by

$$
\begin{aligned}
h_n(t) &= \frac{s_n(t)}{v_f} \quad \text{if} \quad S_1 \le s_n(t), \\
&= h_1 \quad \text{if} \quad 0 \le s_n(t) < S_0.
\end{aligned}
$$

When $s_n(t)$ is between S_0 and S_1, $h_n(t)$ can take either h_1 or $\frac{s_n(t)}{v_f}$.

The rule guiding the choice of the $h_n(t)$ in the transition region is established as follows

$$
\begin{aligned}
h_n(t) &= \frac{s_n(t)}{v_f} \quad \text{if} \quad S_0 \le s_n(t) < S_1, \quad \text{and} \quad v_{n-1}(t) = v_f \\
&= h_1 \quad \text{if} \quad S_0 \le s_n(t) < S_1, \quad \text{and} \quad v_{n-1}(t) < v_f
\end{aligned}
$$

where $v_{n-1}(t)$ is the speed of the leader at time t. This selection rule is postulated based on the observation that drivers can accept increasingly smaller headways in free-flow, but leaves a jam with larger headways until they reach free-flow speeds. One of the consequences of this selection rule is that traffic, once collapsed from free-flow condition, can never regain the maximum flow rate unless new vehicles are inserted into it from on-ramps or other types of sources.

Model C produces a fundamental diagram shown in Fig. 7(b), which resembles the mirrored image of the reversed λ postulated by Koshi et al. [14] (Fig. 1(a)) and the Line-J diagram of Kerner without the scatter ((Fig. 1(b))). Here we note that the corresponding fundamental diagram of Model C would be curved if Line C is slanted. In fact, one can go further with this model. If one modifies the $h_n(t)$ function in the way shown in Fig. 7(c), one obtains the fundamental diagram used in Daganzo's new behavioral traffic flow theory [5](Fig. 7(d)). This is another piece of evidence of the versatility of the new car-following theory.

3.4　Model D

Model D is the most complicated among the four cases that we are discussing in this paper. Its response time function $h_n(t)$ varies according to both spacing and traffic phases, namely acceleration, deceleration and coasting. This function is shown schematically in Fig. 8(a), with parameters (h_0, s_0), (h_2, s_2), (h_3, s_3), and v_f. Here the upper horizontal line is the response time function for the acceleration phase, the lower horizontal line is the response time function for the deceleration phase, and the slanted line is the response time function for the free-flow (coasting phase). Coasting also occurs on any ray passing through the origin and intersects with one, two or all three of the aforementioned lines. For demonstration purposes response time functions for the acceleration and deceleration phases are assumed to be constants, but there's no reason that we cannot make them change with spacing if experimental evidence supports it.
$h_n(t)$ is obtained by below equations.

$$
\begin{aligned}
h_n(t) &= h_3 \quad && \text{for acceleration phase} \\
&= h_2 \quad && \text{for deceleration phase} \\
&= s_n(t)/v* \quad && \text{for coasting phase}
\end{aligned}
$$

Here, acceleration, deceleration, and coasting phases are defined as in Table 1. For the coasting case, $v*$ is $v_n(t)$ when $v_n(t) < v_f$ and $v_{n-1}(t) < v_f$, and $v*$ is v_f, otherwise. The

coasting defined for the case $v_n(t) < v_f$ and $v_{n-1}(t) < v_f$ represents the transition phase between acceleration and deceleration. It happens on a section of a ray passing through the origin and intersects with deceleration and acceleration line of h-S diagram e.g. the line $q' - q''$ in Fig. 8 (a). This transitional coasting is required for the stability of the traffic. To illustrate, if a vehicle changes its response time from h_3 to h_2 shortly after the leader has decelerated and accordingly the spacing has decreased, its new speed may increase because h_2 is less than h_3. This phenomenon (the follower accelerates while the leader decelerates) is against what the real traffic behaves. Thus the transitional coasting is required for the follower to get short enough spacing to decelerate. This is also true for the case the vehicle changes its phase from deceleration to acceleration. We shall use an example to explain how traffic changes phases. Suppose that traffic was initially at point q (Fig. 8(a)) and at time $t > 0$ the leader decelerated to speed v'. How does the follower respond to this change? We postulate that the follower first travels with speed v_f till his spacing gap reduces to S_2, then he steps on his brakes and reduces his speed to v' along the h_2 line. If the leader does not change his speed further, the follower will continue to travel at speed v' and traffic will stay at point q'. Now suppose that the leader accelerates to speed v_f. This time the follower will respond in this way: he first travels at speed v' until the spacing increases to S_a, then he accelerates to speed v_f along the h_3 line, and the traffic will eventually settle at point q'''. As in Model C, traffic can never reach point q or the lower tip of the slanted line (maximum flow point) again unless new vehicles enters the traffic stream.

The fundamental diagram that Model D produces is shown in Fig. 8(b). It captures both the capacity drop and traffic hysteresis. While its hysteresis structure is similar to that in Newell [17], this model has two capacity drops—one occurs at the onset of congestion and the other at the end of recovery from congestion.

All in all, we have shown through the four cases that the specification of (8) is rather general and versatile. This, however, is not our main message here. The key point of the case analyses is that features such as capacity drop and hysteresis are results of driver behavior variability across traffic phases. A theory that models these features must therefore consider this dependence, as we did in our new car-following theory.

4 SIMULATION

The new car-following theory can be easily programmed and simulated on a computer. While the qualitative analysis of the above section tells us the steady state relations between its variables (i.e., flow, density, speed), traffic simulations allow us to study the transient behavior of this new theory. We shall conduct the simulation on a ring road, which simplifies the analysis a great deal because we do not have to specify boundary conditions. The general parameters used to simulate traffic are as follows. The length of the ring road is 1080m, the length of a vehicle is 6m, its maximum travel speed is 30m/sec(108km/hr) (Fig. 9), and the simulation is updated every1 second. The specific parameters related to each models are as follows: Model B—S_0=30m, h_0=1sec; Model C— S_0=30m, S_1=45m, h_0=1sec, h_1=1.5 sec; and Model D— S_0=30m, S_2=36m, S_3=54m, h_0=1sec, h_2=1.2sec, h_3=1.8sec. A free flow speed v_f of 30m/sec is used for all models.

We start with an empty ring road and fill it with vehicles gradually. A vehicle enters or exits the ring road one by one for every 20 seconds. An entering vehicle always joins the tail of a platoon while a leaving vehicle can exit from any location because it is randomly chosen from the platoon. A total of 180 vehicles (1080/6) is needed to jam the ring road,

but we only release 85 vehicles onto the ring road in the aforementioned manner. Moreover, we place three detectors located at 270m, 540m and 810m respectively (see Fig. 9). Each of the detectors is 40m long and measures traffic density and space-mean travel speeds. Here density is defined as the number of the vehicles on the detector divided by the length of the detector at each simulation time step, and speed is defined as the arithmetic mean of the speeds of those vehicles that are on the detector during each simulation time step. These quantities are then averaged over the detector polling intervals, that is, every 20 seconds. Flow is then computed using the fundamental relation

$$q = \rho v.$$

The simulation results are shown in Fig. 10-12. In Fig. 10, the speed measured from detector B for Model B simulation is shown in the upper right corner (measurements from detectors A and C are similar to that of detector B and is therefore not shown here), which shows a prolonged period of congestion. The flow-density plot of the measured data, shown in the up left corner, has a triangular shape, which is what it should be. Although there are small oscillations shown in the speed-time plot, these oscillations do not profess in the flow-density plot, perhaps due to averaging and the way flow rate is computed. These small oscillations are completely suppressed in the lower plots where traffic speed and density are averaged over the entire ring road, using the ring road itself as a giant detector.

Fig. 11 shows the simulation results for Model C. On the left are the flow-density plots for the three detector locations and the entire ring road., and on the right are the respective time-speed plots. One should note that the flow-density plots produced show the reversed-λ image. Yet there are subtle differences between these plots. The differences occur in traffic regions where sharp phase transitions took place (circled area on the right plots). First note that the small oscillation detected at A was magnified when it went through detectors B and C. Next the time trajectory of phase transitions on the left plots (the thin arrowed lines) shows clearly the sudden drop of flow rate during a free-flow–congested-flow transition, and is very indicative of the so-called fast-waves suggested in Daganzo's behavioral traffic theory [5].

In Fig. 12, the simulation results of model D are drawn. Again only measurements from detector B are used because those from other detectors are similar. The flow-density phase plots show three things: 1) capacity drop, 2) hysteresis loops (thin arrowed lines), and 3) fast-waves (during transition from free-flow to congested flow).

5   CONCLUDING REMARKS

Capacity drop and hysteresis are two prominent features of multi-phase vehicular traffic flow, which are believed to be related to drivers' behavioral shifts during phase transitions. Yet current car-following theories model vehicular traffic as a homogeneous process comprising a single phase, preventing them from capturing the aforementioned traffic features. In this paper a new car-following model is proposed and discussed. It proposes that drivers adopt a speed of travel according to their front spacing and response times. Moreover, driver response time is assumed to be a function of both vehicle spacing and traffic phase. By specifying various functional forms of response time, one obtains specific cases of the general car-following theory, some of which can model capacity drop (Model C) and/or traffic hysteresis (Model D) while others are shown to be equivalent of well-know existing theories (e.g., Model B).

Both theoretical analsyses and numerical simulations have demonstrated the potential of the new car-following theory to model complex traffic patterns. Further research to analyze its stability property and obtain its parameters from experimental data is underway. It is hoped that this new theory, once validated, can provide a more realistic and powerful traffic flow model for high fidelity microscopic traffic simulations.

Acknowledgements

References

[1] Bando, M., Hasabe, K., Nakayama, A., Shibata, A., Sugiyama, Y. (1995). Dynamical model of traffic congestion and numerical simulation, *Physical Review E, Vol.51 No.2*, pp.1035-1042.

[2] Chandler R.E., Herman, R., and Montroll E.(1958). Traffic Dynamics: Studies in Car Following, *Operations Research, Vol 6*, pp.165-184.

[3] Edie, L.C. and Foote, R.S. (1958). Traffic Flow in Tunnels. *Highway Research Board Proc. Vol. 37*, pp.334-344.

[4] Edie, L. C. (1961). Following and Steady-State Theory for Non-congested Traffic, *Operations Research, Vol .9*,pp.66-76.

[5] Daganzo, C.F. (1999). A behavioral Theory of Multi-Lane Traffic Flow Part I: Long Homogeneous Freeway Sections. *UCB-ITS-RR-99-5*, ITS UCB.

[6] Del Castillo, J.M. and F.G. Benitez (1995), On functional form of the speed-density relationship—I: general theory, II: empirical investigation. *Transp. Res. 29B*, 373-406.

[7] Drake, J.S., Schofer, J.L., and May, A.D.,(1967). A Statistical Analysis of Speed Density Hypothesis. *Highway Research Record 154*, pp. 53-87.

[8] Forbes, T.W. (1963). Human Factor Considerations in Traffic Flow Theory. *Highway research Board, Record 15*, pp. 60-66.

[9] Gazis, D.C., Herman, R., and Potts, R.B.(1959). Car-Following Theory of Steady-State Traffic Flow. *Operations Research, Vol 7*,pp. 499-505.

[10] Gazis, D. C., Herman, R., and Rothery, R. W.(1961). Nonlinear Follow-the-leader Models of Traffic Flow, *Operations Research, Vol 9*, pp.545-567.

[11] Greenberg, H. (1959). An Analysis of Traffic Flow, *Operations Research, Vol 7*,pp.79-85

[12] Greenshields, B. D. (1934). A Study of Traffic Capacity. *Proc. Highway Research Board Vol. 14.*, pp.448-477.

[13] Kerner, B.S. (1998) Experimental features of self-organization in traffic flow,*Physical Review Letters Vol. 81, No. 17*, pp.3797-3800.

[14] Koshi, M., Iwasaki, M., Ohkura, I. (1983). Some Findings and an Overview on Vehicular Flow Characteristics, *Proc. 8th Intl. Symp. on Transportation and Traffic Flow Theory*(V. Hurdle, E. Hauer, G. Stuart ed.) pp. 403-426.

[15] Maes, W. (1979) Traffic data collection system for the Belgian motorway network—measures of effectiveness aspects. *Proceedings of the International Symposium on Traffic Control Systems*, Vol. 2D—Analysis and Evaluation, pp. 45–73.

[16] Newell, G.F.(1961). Nonlinear Effects in the Dynamics of Car Following, *Operations Research, Vol 9*, pp.209-229.

[17] Newell, G.F. (1965). Instability in Dense Highway Traffic, a Review. *Proc. 2nd Intl. Symp. on the Theory of Road Traffic Flow*,(J. Almond ed.), Paris, pp. 73-83.

[18] Newell, 1999, A simplified car-following theory: a lower order model, Research Report UCB-ITS-RR-99-1, Institute of Transportation Studies, University of California at Berkeley

[19] Pipes, L.A. (1953). An Operational Analysis of Traffic Dynamics. *Journal of Applied Physics, Vol. 24 No. 3*, pp. 274-281.

[20] Treiterer, J. and Myers, J.A. (1974). The Hysteresis Phenomenon in Traffic Flow. *Proc. 6th Intl. Symp. on Transportation and Traffic theory*, (D.J. Buckley ed.), pp. 13-38.

[21] Zhang, H.M.(1999). A mathematical theory of traffic hysteresis, *Transportation Research* Part B 33, pp. 1-23.

Table 1: Definition of Coasting(C), Acceleration(A), and Deceleration(D)

	$v_n(t) = v_f$	$v_n(t) < v_f$
$v_{n-1}(t) = v_f$	$s_n(t) \geq S_0$: C $s_n(t) < S_0$: D	$s_n(t) \geq S_3$: C $s_n(t) < S_3$: A
$v_{n-1}(t) < v_f$	$s_n(t) \geq S_2$: C $s_n(t) < S_2$: D	$s_n(t) \geq v_n(t) \cdot h_3$: A $s_n(t) \leq v_n(t) \cdot h_2$: D $v_n(t) \cdot h_2 < s_n(t) < v_n(t) \cdot h_3$: C
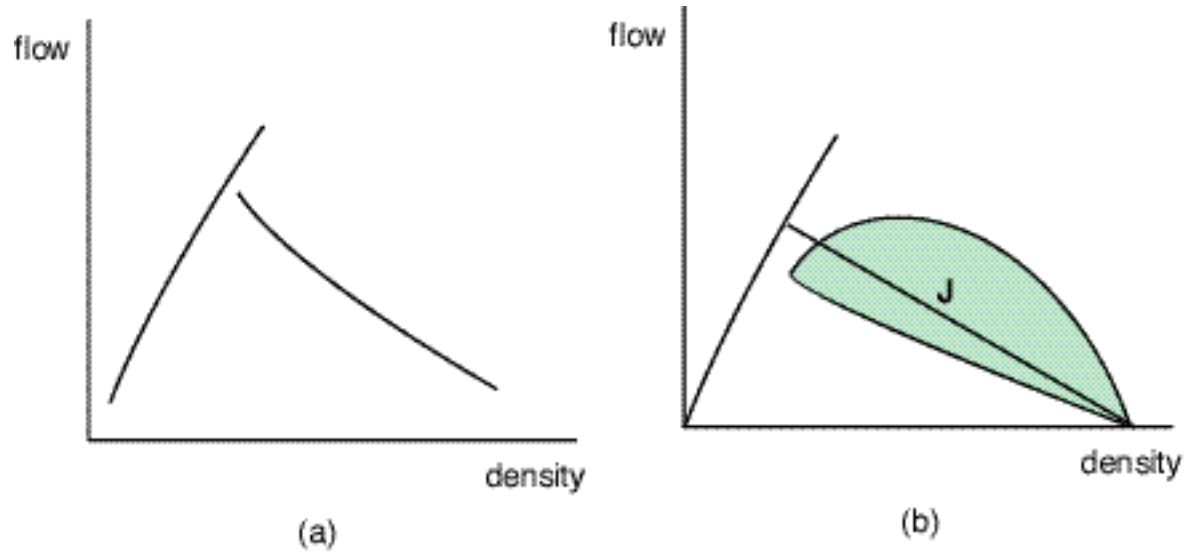
Figure 1.   Fundamental diagram proposed by (a) Koshi et al. (1983) and (b) Kerner (1998). The line J in (b) represents the characteristics of the downstream of a wide jam not a part of fundamental diagram. (reproduced)
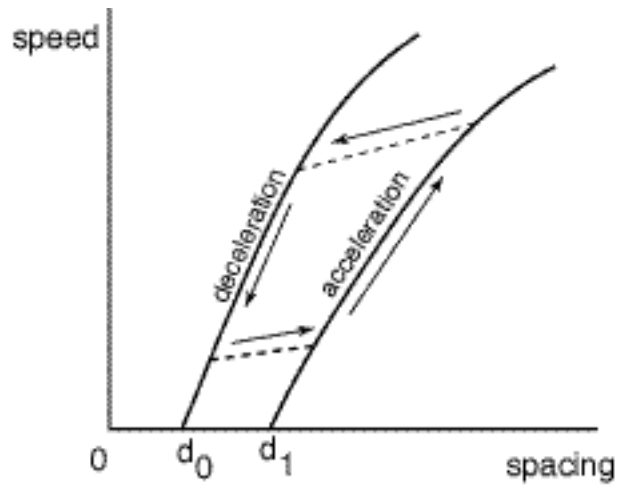
Figure 2. Speed-spacing relationship proposed by Newell (1965)
(reproduced)
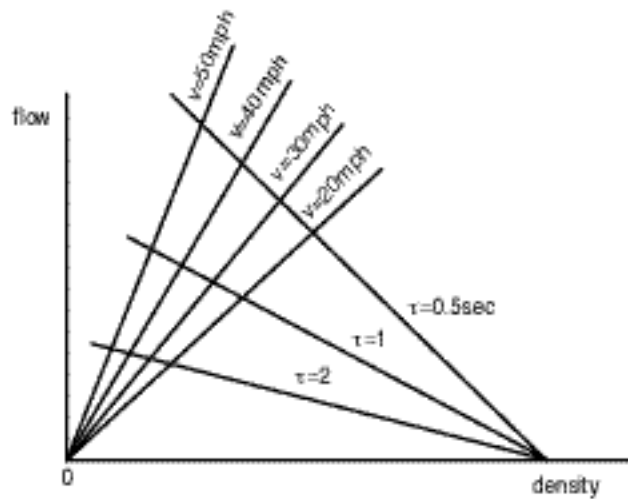
Figure 3. flow-density relationship for various time
gap and speed Forbes (1963) (reproduced)

(a) h-S relationship

(b) Fundamental diagram
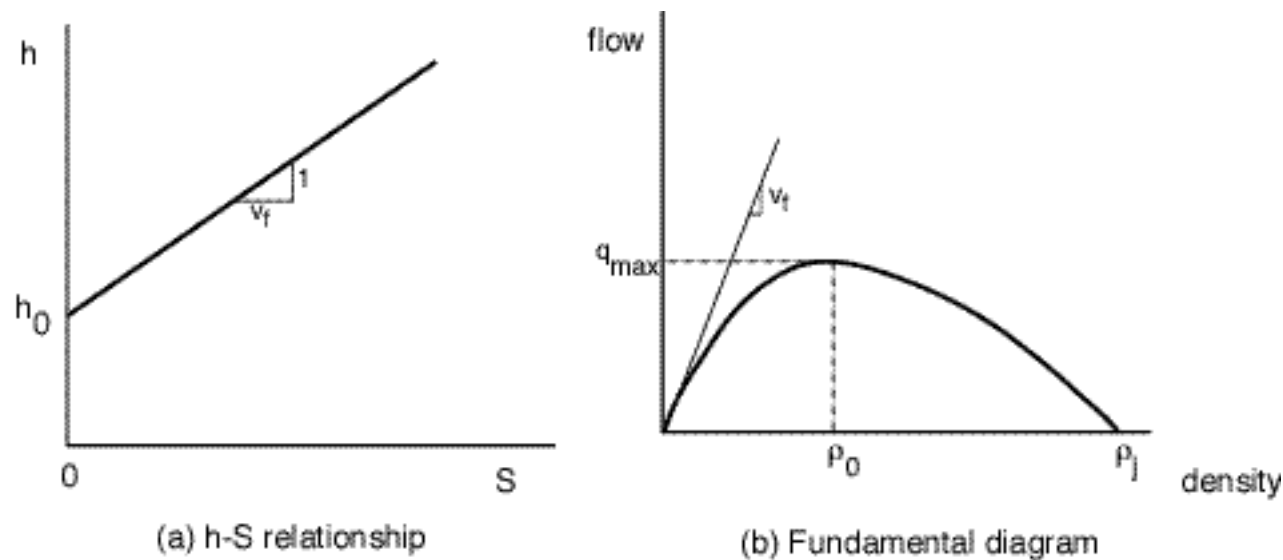
Figure 4. Description of Model A
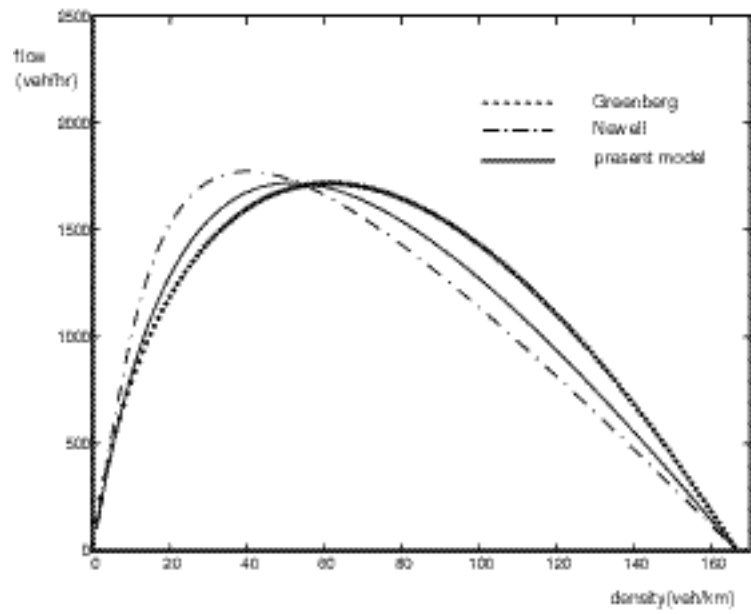
Figure 5. Comparison of fundamental diagram.

(a) h-S relationship

(b) Fundamental diagram
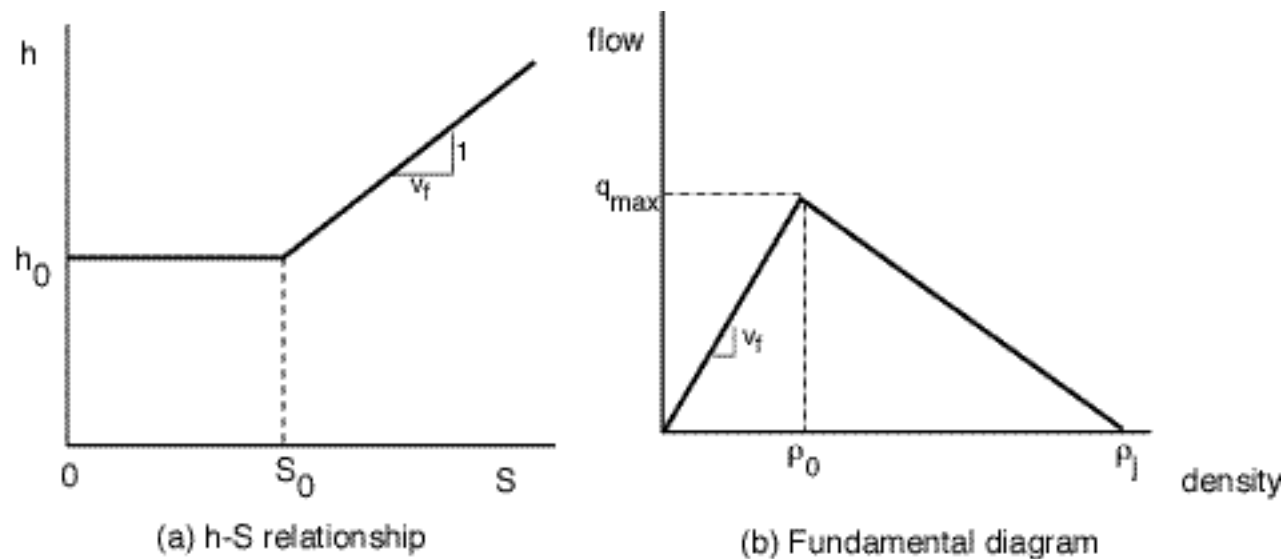
Figure 6. description of Model B
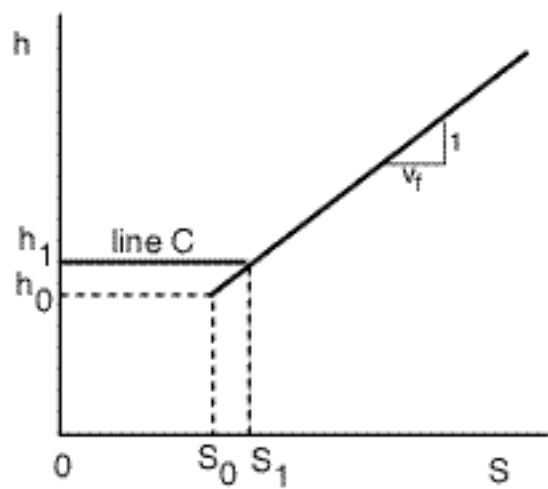
(a) h-S relationship
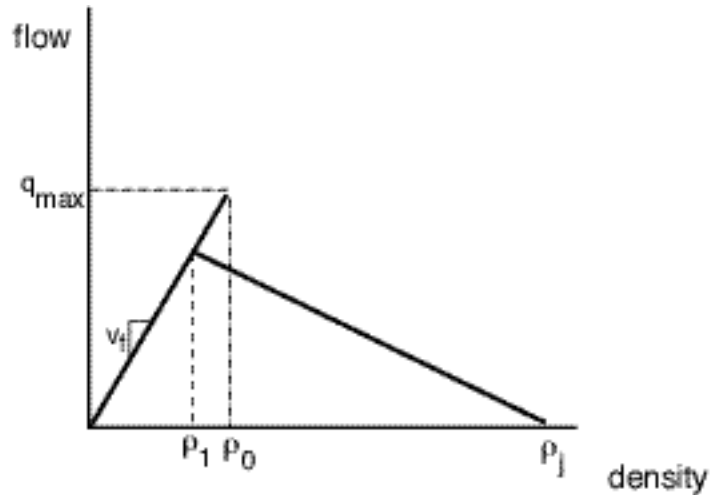
(b) Fundamental diagram
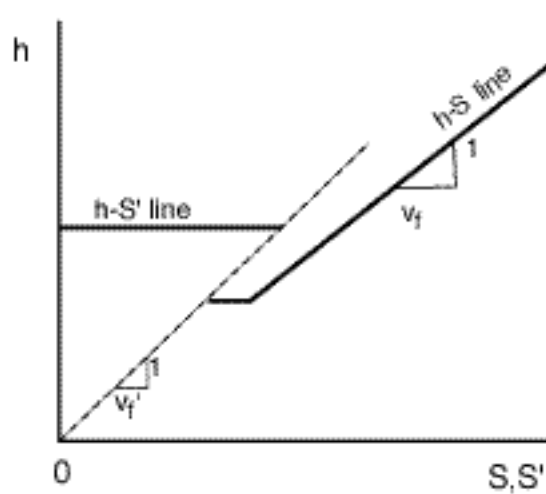
(c) adjusted h-S relationship
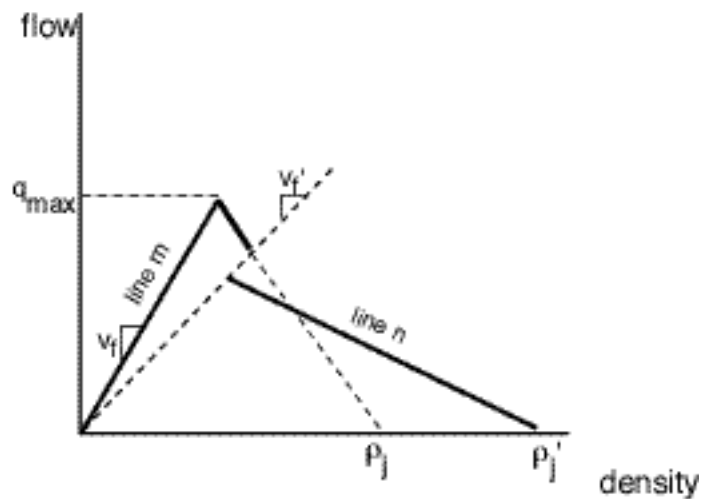
(d) Daganzo's Fundamental diagram (1999) (reproduced)

Figure 7. Description of Model C

(a) h-S relationship

(b) Fundamental diagram
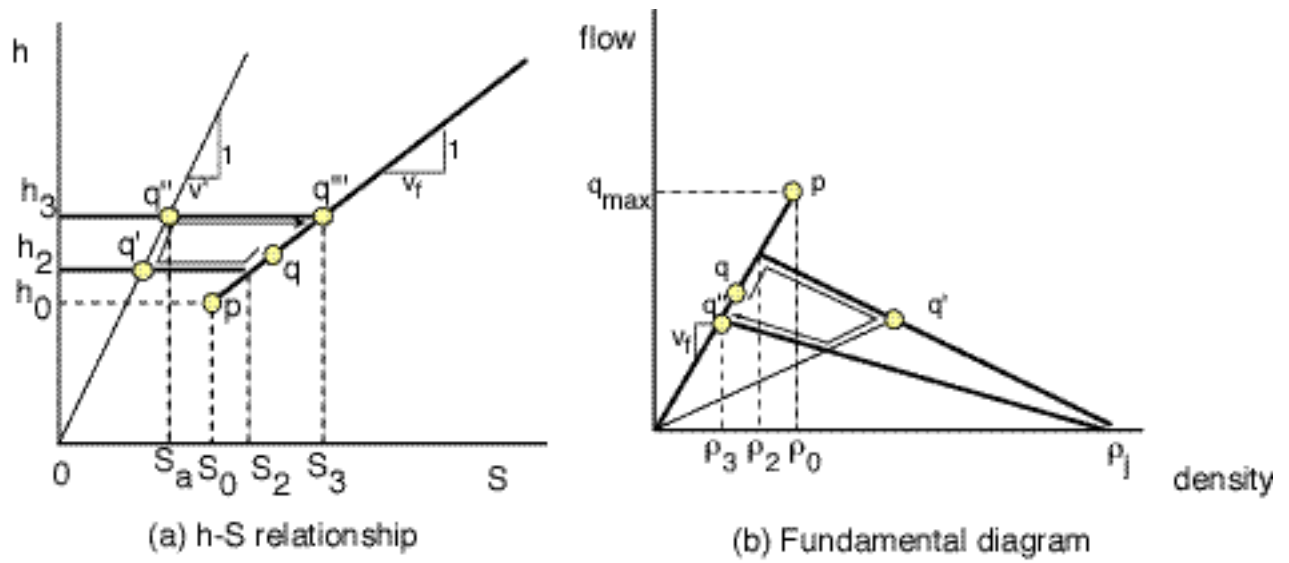
Figure 8. Description of Model D
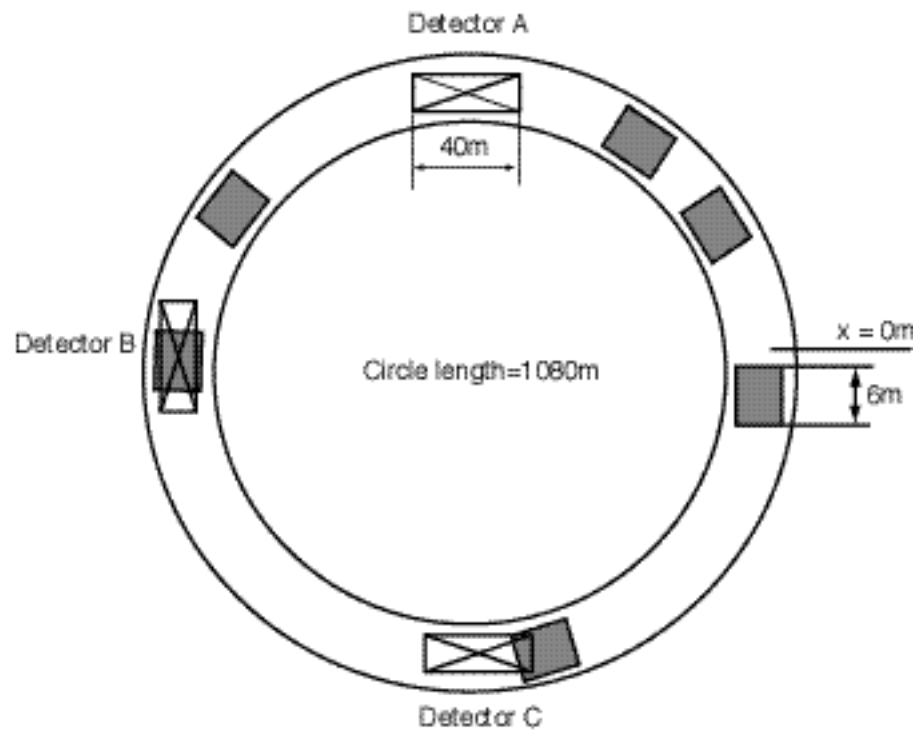
Figure 9. Configuration of simulation field
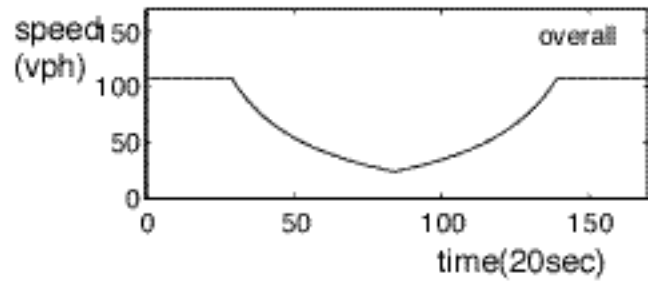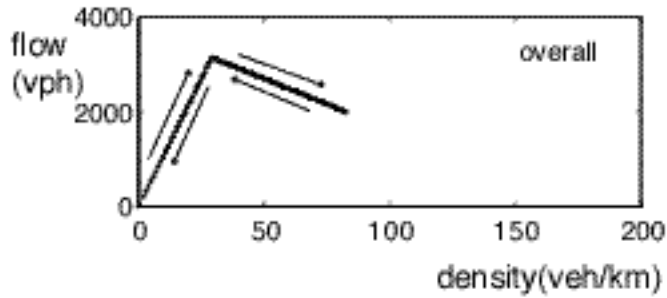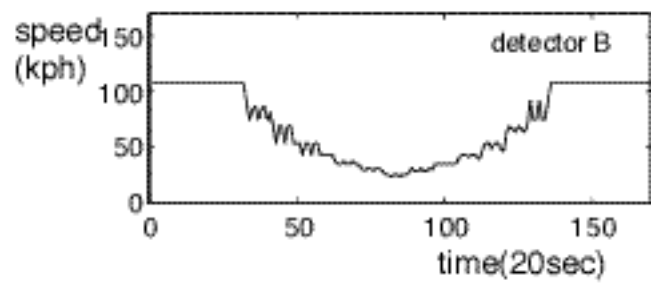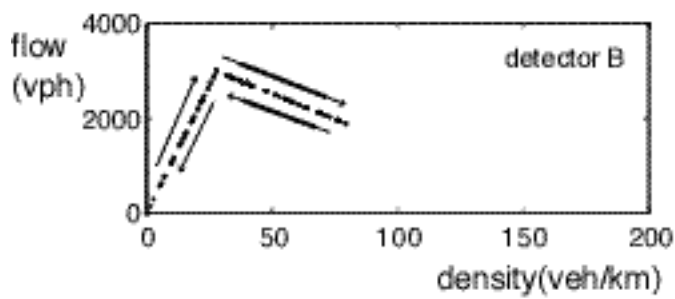
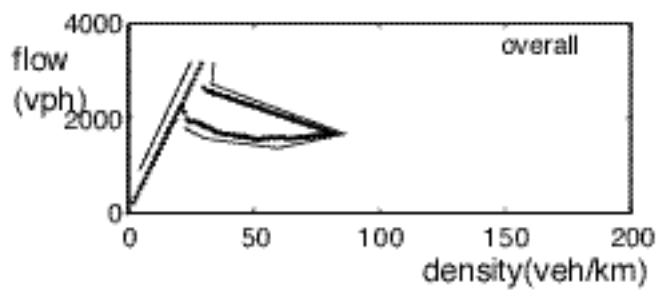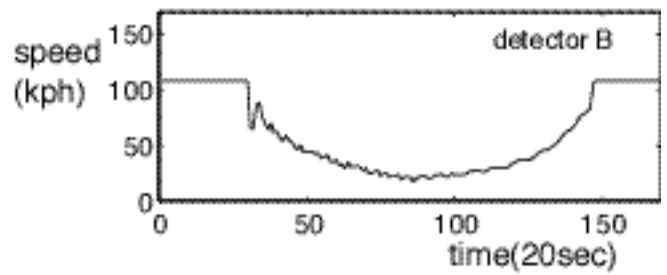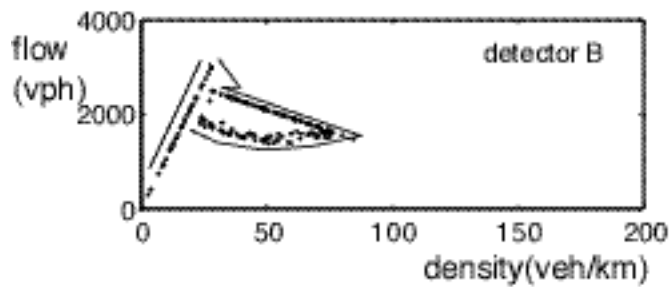Figure 10. Simulation result of Model B
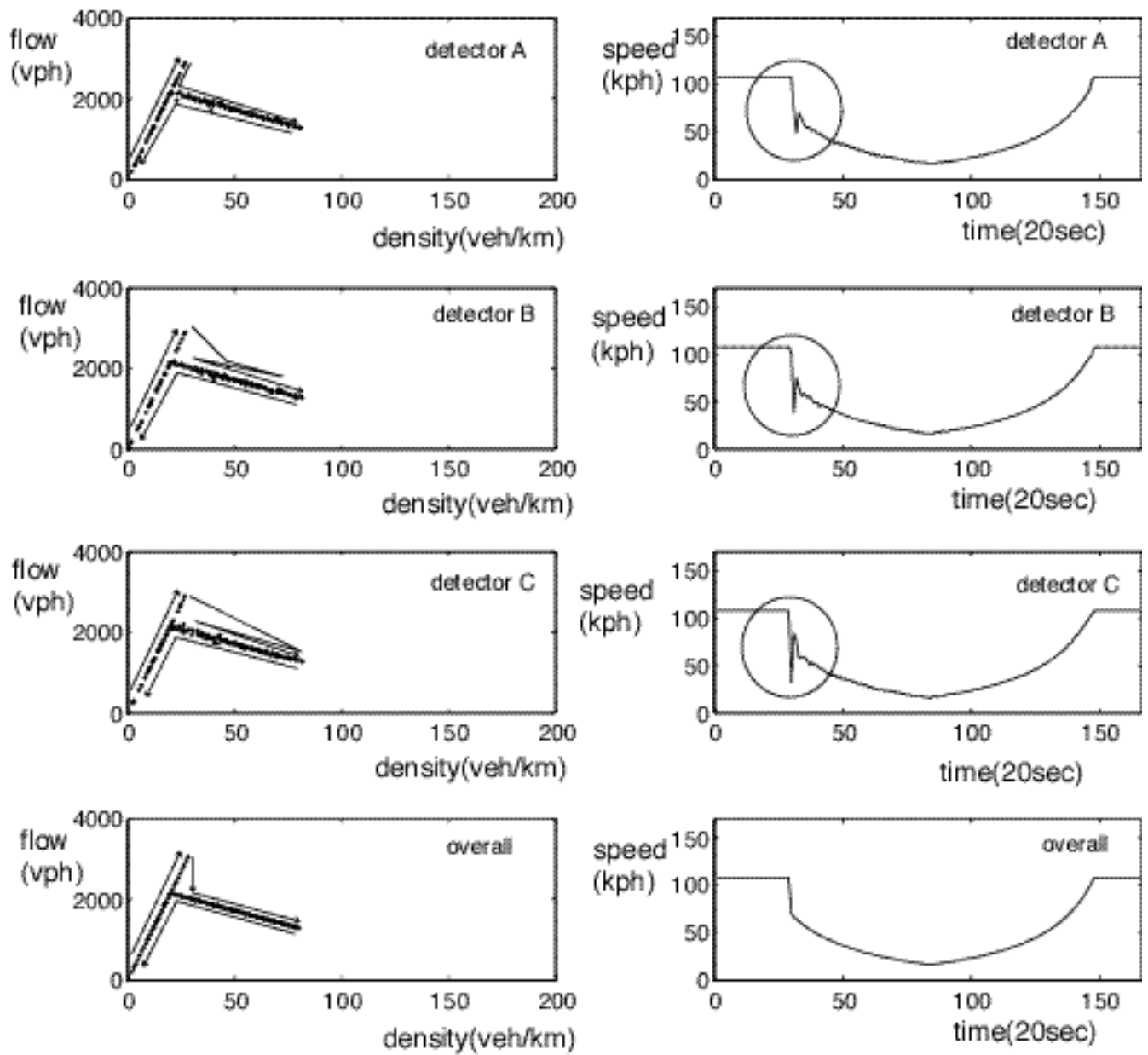
Figure11. Simulation result of ModelC
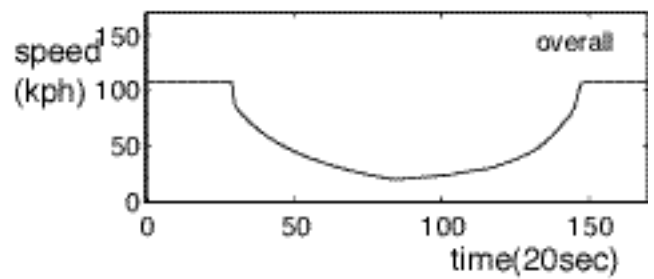
Figure12. Simulation result of ModelD